

Molecular Simulation

ISSN: 0892-7022 (Print) 1029-0435 (Online) Journal homepage: www.tandfonline.com/journals/gmos20

Molecular dynamics and integral equation study of the structure and dynamics of solid and liquid magnesium phosphide

Yenal Aydın, Seçkin D. Günay, Ünsal Akdere & Çetin Taşseven

To cite this article: Yenal Aydın, Seçkin D. Günay, Ünsal Akdere & Çetin Taşseven (2024) Molecular dynamics and integral equation study of the structure and dynamics of solid and liquid magnesium phosphide, Molecular Simulation, 50:1, 1-8, DOI: 10.1080/08927022.2023.2267681

To link to this article: https://doi.org/10.1080/08927022.2023.2267681

Published online: 17 Oct 2023.

Submit your article to this journal

Article views: 125

View related articles

View Crossmark data

Citing articles: 1 View citing articles

Full Terms & Conditions of access and use can be found at
https://www.tandfonline.com/action/journalInformation?journalCode=gmos20

MOLECULAR SIMULATION
2024, VOL. 50, NO. 1, 1–8
https://doi.org/10.1080/08927022.2023.2267681

Taylor & Francis
Taylor & Francis Group

Check for updates

Molecular dynamics and integral equation study of the structure and dynamics of solid and liquid magnesium phosphide

Yenal Aydın[a,b], Seçkin D. Günay[a], Ünsal Akdere[a] and Çetin Taşseven[a]

[a]Department of Physics, Yıldız Technical University, İstanbul, Turkey; [b]Goztepe MedicalPark University Hospital, İstanbul, Turkey

ABSTRACT

The static structure and self-ionic transport in solid and molten magnesium phosphide (Mg_3P_2) are investigated by means of the molecular dynamics simulation and the hypernetted-chain theory of liquids using a newly developed semiempirical pairwise potential. Parameters of the potential were fitted to the lattice constant and bulk modulus, and then it was tested in NVE ensemble simulation at 300 K at which X-ray powder diffraction pattern was correctly reproduced. The static structure and the dynamics of self-ion transport were investigated in NPT simulations between 300 and 1500 K. The temperature evolution of the radial distribution functions, coordination numbers, mean square displacements, self-diffusion coefficients and solid–liquid transition were established at solid and liquid phases that will be informative for the thermoelectronic, optoelectronic and energy storage applications of the magnesium phosphide.

ARTICLE HISTORY
Received 19 July 2023
Accepted 26 September 2023

KEYWORDS
Magnesium phosphide; model potential; static and dynamic properties; molecular dynamics simulation; hypernetted-chain theory

1. Introduction

As being one of the members of the magnesium pinictides (Mg_3Pn_2), magnesium phosphide (Mg_3P_2) is also considered as potential candidate material for thermoelectronic and optoelectronic device development due to its extraordinary electronic properties [1–3]. One of the first principle calculations on Mg_3P_2 assessed that it is a suitable material for such applications due to its the structural, electronic, optical and thermoelectric properties, while another shows that there exist four stable phases from ambient conditions up to 100 GPa [1,2]. At low temperatures, Mg_3P_2 exhibits the characteristics of a semiconductor material with a direct band gap of 1.73 eV [4]. It has a cubic antibixbyte structure with $Ia\bar{3}$ symmetry group forming a unit cell which contains 32 phosphorus atoms and 48 magnesium atoms [5,6]. Despite the possibility that magnesium phosphides may be a suitable material for the production of thermoelectric and optoelectronic devices, to the best of our knowledge, there are very limited theoretical or experimental studies on its thermophysical properties. This work aims to clarify the structural and ionic transport properties such as local ionic order and ionic diffusion of Mg_3P_2 at liquid and solid phases through constant pressure-temperature (NPT) atomistic simulation in conjunction with a newly developed classical pairwise additive potential. Moreover, Hypernetted-Chain (HNC) theory of liquids is also used to investigate liquid state structure above the melting point.

2. Methodology

2.1. Molecular dynamics simulation

The molecular dynamics (MD) simulations were conducted in the NVE (constant Number, Volume and Energy) and the isobaric-isothermal NPT (constant Number, Pressure, and Temperature) ensembles. The simulation box of $4\times4\times4$ was constructed by setting 3072 Mg^{+2} atoms and 2048 P^{-3} atoms according to $Ia\bar{3}$ space group with cubic antibixbyte structure specified by Wyckoff positions [6]. The long-range Coulomb interactions are managed using The Ewald's sum method [7] with cutoff radius $r_c = 20$Å. The periodic boundary conditions were applied on the simulation cell to avoid the surface effects. The Beeman's predictor–corrector method was applied to solve Newton's equation of motion to compute the positions and velocities of the ions with the time step of $\Delta t = 0.001$ ps with a total run time of 100 ps. The first 30 ps is to reach the desired equilibrium state, then the physical properties were calculated by averaging over the following 70 ps. Nosé–Hoover thermostat and Parrinello–Rahman constant stress method [7,8] were applied in order to control the temperature and pressure. The MD simulations have been performed in NVE ensemble at 300 K and NPT ensemble in the range of 300 to 1500 K at 50 K intervals.

2.2. Liquid state theory-HNC approximation

Ornstein–Zernike (OZ) integral equation relates the total correlation function $h_{ij}(r)$ and direct correlation functions $c_{ij}(r)$ for a homogeneous and isotropic binary liquid system with ionic components i and j [9],

$$\gamma_{ij}(r) \equiv h_{ij}(r) - c_{ij}(r) = \sum_l n_l \int d\vec{r}\, c_{ij}(|\vec{r} - \vec{r}'|) h_{ij}(\vec{r}') \quad (1)$$

The liquid state approximate closures aim to solve OZ integral equation by relating the direct correlation function $c_{ij}(r)$ and the radial distribution function $g_{ij}(r)$ via the electrostatic pair potential $\phi_{ij}(r)$. One of the well-known approximate closures

CONTACT Çetin Taşseven tasseven@yildiz.edu.tr
© 2023 Informa UK Limited, trading as Taylor & Francis Group

Table 1. Values for the potential parameters as the strength $A_{i,j}$, hardness $\rho_{i,j}$, van der Walls $C_{i,j}$ and screening $\lambda_{i,j}$(Å).

Ion pair	$A_{i,j}$(eV)	$\rho_{i,j}$(Å)	$C_{i,j}$ (eVÅ^6)	$\lambda_{i,j}$(Å)
Mg–Mg	1.62×10^4	0.105	0	0
Mg–P	2.40×10^4	0.217	36.4	1.0
P–P	5.22×10^2	0.578	572.87	3.0

The effective charges are $Z_{Mg} = +1.10$ and $Z_P = -1.65$.

Table 2. The lattice constant and the mechanical properties of Mg_3P_2in units of GPa at $T = 0$K calculated using the general utility lattice program (GULP) [12].

Properties	This work	Experiment/First principal
a_0 (Å)	11.92	12.01 [4], 12.00 [6], 12.006 [1]
K	59.87	59.78 [1], 58.92 [13]
G_V, G_R, G_H	33.23, 32.65, 32.94	
E	72.69	
C_{11}, C_{12}, C_{44}	97.22, 41.20, 36.70	
υ	0.29	

is called hypernetted-chain approximation,

$$c_{ij}(r) = g_{ij}(r) - 1 + \frac{1}{k_B T}\phi_{ij}(r) + ln[g_{ij}(r)] \tag{2}$$

where $g_{ij}(r) = h_{ij}(r) - 1$. Picard and Newton–Robson combined iteration method, which was proposed by Gillan [10] and Abernethy-Gillan [11], has been used to solve the OZ integral equation. We solve the mean spherical approximation (MSA) [9] with charged hard-spheres for the initial estimation of the function $\gamma_{ij}(r)$. The accuracy of the solution at each stage has been taken as $|\gamma_{ij}^{k+1}(r) - \gamma_{ij}^{k}(r)| < 10^{-4}$. This method leads to an accurate numerical solution of the OZ equation in about 20–30 iterations. $M = 2048$ mesh point has been used for each run by cooling down the system gradually from an initial temperature T_i to the desired temperature T_f. Mesh length, namely displacements, in real and reciprocal space is adjusted using $\Delta r \Delta k = 2\pi/M$.

2.3. Pair potential

Buckingham type of rigid ion potential has been used to model the short range of interactions between the ionic species in addition to the long-range Coulomb interaction, $Z_i Z_j/r$. The pairwise short-range potential is simply described by a repulsive exponential term and an attractive term known as van der Walls interactions [12]

$$\phi_{ij}^{s}(r) = A_{ij}\exp\left(-\frac{r}{\rho_{ij}}\right) - \frac{C_{ij}}{r^6} \tag{3}$$

where A_{ij}, ρ_{ij} and C_{ij} are the strength, hardness and van der Walls parameters, respectively, and Z_{ij} is the effective charge.

3. Results and discussion

3.1. Development of the pair potential

Commonly known trial and error method has been used to estimate the potential parameters A_{ij}, ρ_{ij}, C_{ij} and Z_{ij}. Lattice constant and bulk modulus of the magnesium phosphide crystal were fitted to available experimental and first principal data by employing the unparametrised functional form of the potential in the general utility lattice program (GULP) [13]. Tables 1 and 2, respectively, show the obtained potential parameters, and the lattice constant, cohesive energy and some mechanical properties. Bulk modulus (K), shear modulus (G_V, G_R, G_H), Young's modulus (E) and Poisson's ratio (v) are calculated using GULP following the Voigt–Reuss–Hill approximation [13].

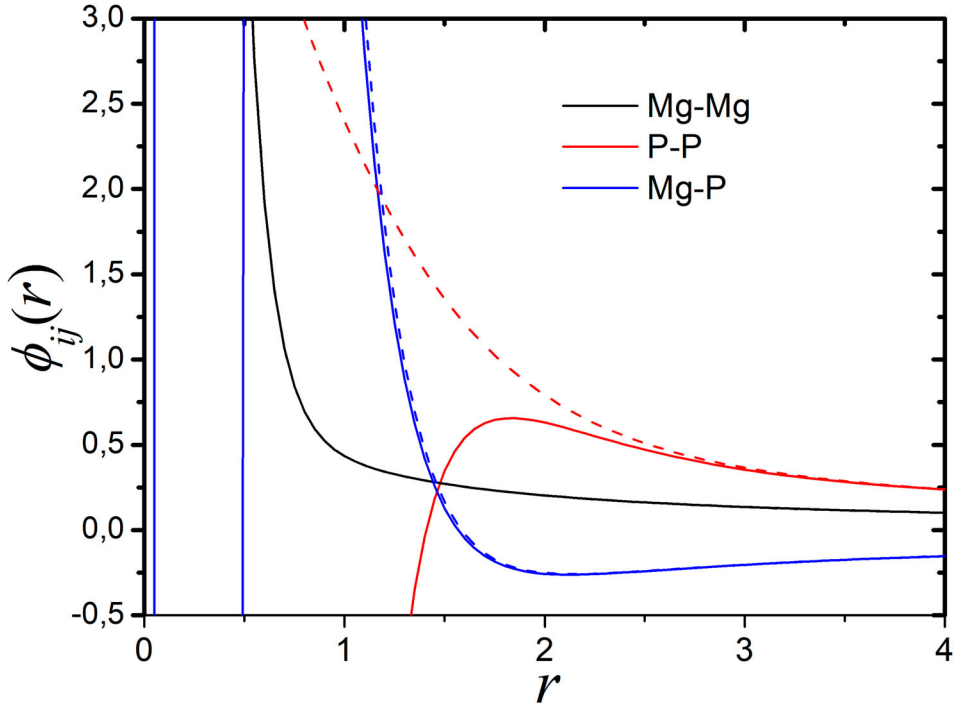


Figure 1. (Colour online) Pair potential for Mg_3P_2 in units of e^2/Å = 14.399 eV. Dashed lines represent the pairwise interactions with the screened van der Walls term.

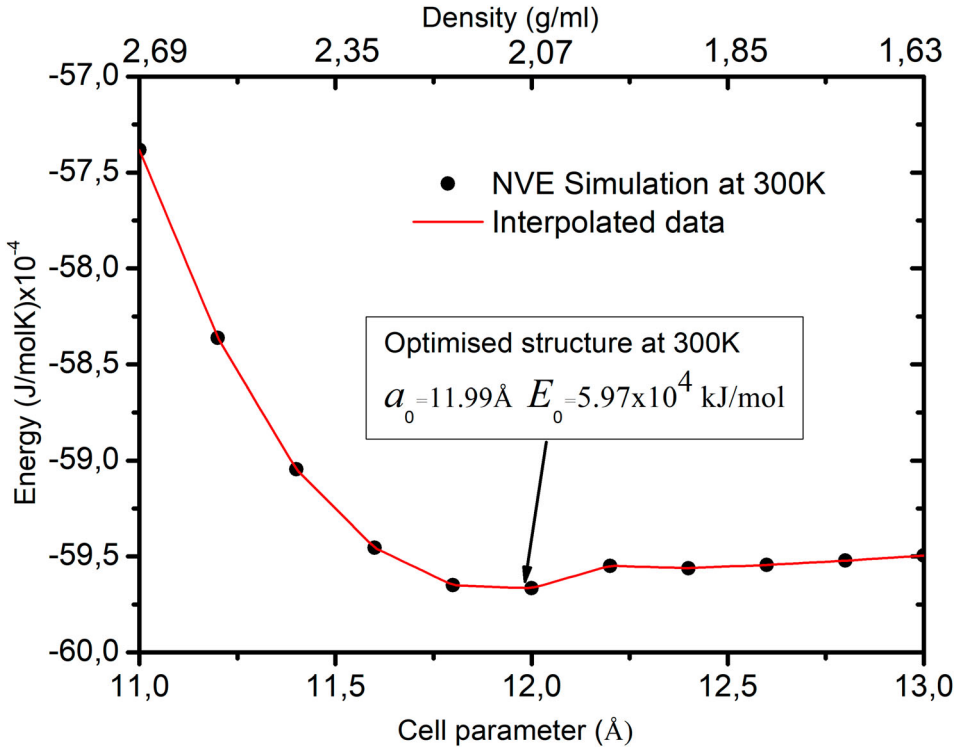


Figure 2. (Colour online) Unit cell energy of Mg_3P_2 versus cell parameter and density at 300 K in microcanonical NVE ensemble.

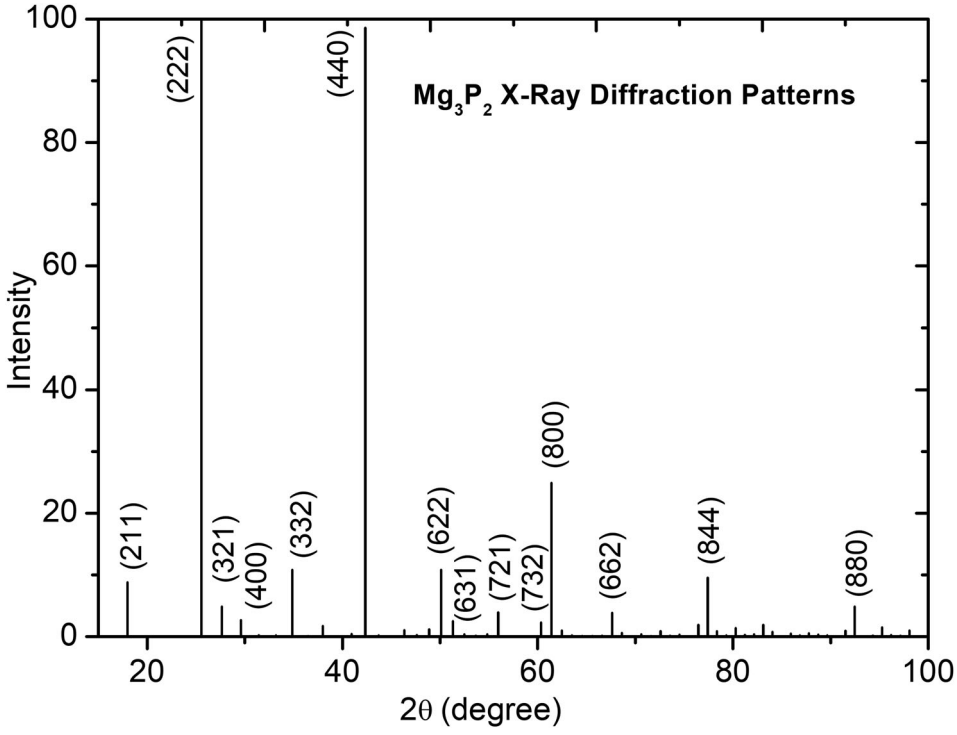


Figure 3. (Colour online) Simulated XRD pattern of magnesium phosphide as intensity versus Bragg angle 2θ (°). The lattice planes are expressed as the Miller indices (*hkl*) for each corresponding crystalline peak.

Figure 1 represents the pair potential developed for Mg_3P_2. It is common that Buckingham form of the potential produces unrealistic attraction at very short regions due to $1/r^6$ van der Walls term. This unrealistic behaviour of the potential can be dealt with in different ways. During the HNC calculations, this problem was handled using an exponential screening term $\exp(-\lambda/r)$. Van der Walls terms for P–P and Mg–P interactions were multiplied by the screening term where the screening parameters were estimated as $\lambda_{PP} = 3.0$Å and $\lambda_{MgP} = 1.0$Å. Corrected interactions are shown with dashed lines in Figure 1.

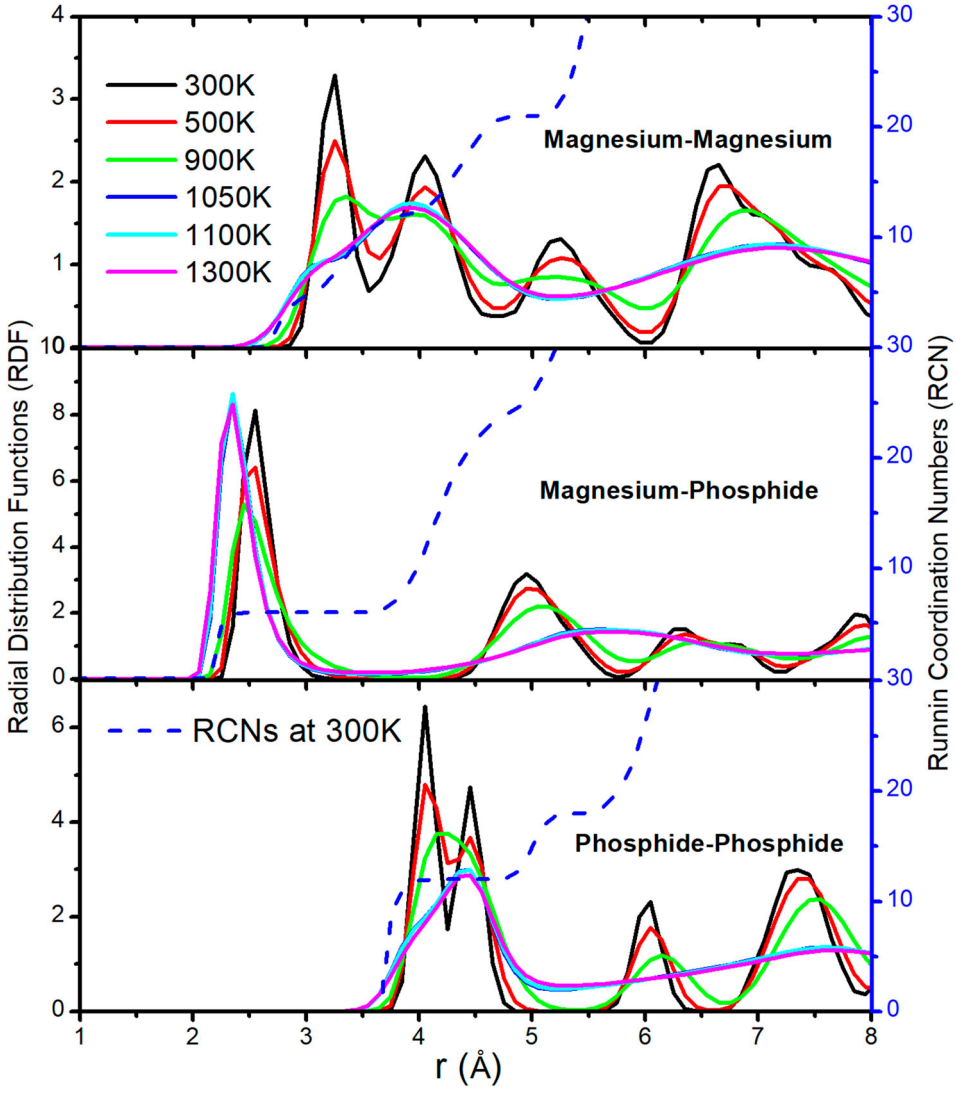


Figure 4. (Colour online) The radial distribution functions $g_{ij}(r)$ of Mg_3P_2 at six different temperatures covering both solid and liquid phases. The running coordination numbers $g_{ij}(r)$ at 300 K are shown as a dashed line.

3.2. NVE ensemble simulation

All MD simulations were performed with MOLDY code [14]. The NVE calculations have been carried out for the cell parameter a_0 varying between 11Å and 13Å with $\Delta a_0 = 0.2$Å at constant temperature $T = 300$K and number of particles $N = 5120$ in the simulation box of size $4a_0$. Volume optimisation was based on the minimisation of the cell energy $\left(\frac{dE}{d\rho}\right)_T = 0$. The cell parameter and density versus energy curve are given in Figure 2. The optimised cell parameter and density are $a_0 = 11.99$Å and $\rho = 2.07$ g/ml, respectively, which agree well with the previous experimental data and first-principles calculations of the lattice parameter of between 12.00Å − 12.01Å [1,4,6], and the density of 2.055 g/ml [15] and 2.1 g/ml [16]. The minimum energy of the optimised cell was obtained as -5.9665×10^4 kJ/mol.

3.3. NPT ensemble simulation and HNC theory

Isobaric-Isothermal ensemble simulations have been performed in order to study the temperature evolution of physical properties of magnesium phosphides between 300 and 1500 K at 50 K intervals and zero pressure. In Figure 3, we present X-ray powder diffraction pattern of Mg_3P_2 using the structural analysis program VESTA [17]. The XRD pattern was developed from the structural data calculated at 300 K in NPT ensemble. The simulated XRD diffractogram peaks with corresponding lattice planes expressed as the Miller indices (hkl) in Figure 3 show that the XRD patterns data from the Materials Project for Mg_3P_2 (mp-2514) [5] was successfully reproduced.

The radial distribution function (RDF), $g(r)$, is a measure of the local order–disorder of the static structure of the system. The running coordination number (RCN) $n(r)$ is calculated by the integration of RDF in spherical coordinates which gives the number of particles in the range of each coordination sphere. Figure 4 shows the radial distribution functions of ionic pairs $g_{ij}(r)$ at six different temperatures covering both solid and liquid phases. The RCNs $n_{ij}(r)$ at 300 K are also presented in Figure 4. Before the principal peak $g_{ij}(r) = 0$ for all ionic pairs as a result of short-range strong repulsive interactions. Fundamentally, the peaks of $g_{ij}(r)$ of an ideal crystal should be in the form of vertical lines for all ranges of r due

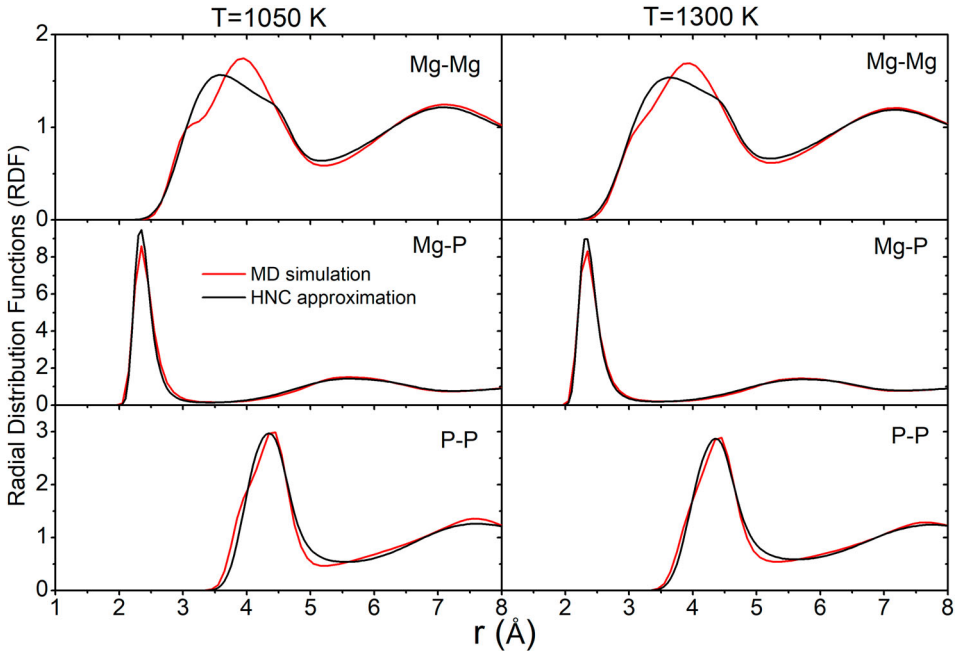


Figure 5. (Colour online) The radial distribution functions $g_{ij}(r)$ of hypernetted-chain approximate theory (black line) and molecular dynamics simulation (red line) $T_f = 1050$K and $T_f = 1300$K.

to long-range order. Because of the thermal vibrations, the uncertainty in the positions of ions is increased and the line becomes peak. As the temperature increases, the peaks are broadened and the height is lowered; however, these peaks are not dissolved and can be easily distinguished one from another up to 1050 K as can be seen from Figure 4. Beyond the 1050 K, although the principal peaks are still visible while the others are destroyed at large separations with less pronounced oscillations about one $\left(\lim_{r\to\infty} g(r) = 1\right)$ as a consequence of lack of long-range ordering, which clearly displays the characteristic features an ionic melt. The first peak positions, which give the average nearest-neighbor separations, do not vary significantly with temperature except that the average separation between magnesium and phosphorus ions is reduced by 7.8% across the melting at about 1050 K. Mg–Mg pairs has wider and lower peaks compare to that of P–P pairs indicating that the magnesium ions exhibit a lower degree of correlation, more pronounced thermal vibrations at solid phase and a greater self-diffusive behaviour at liquid phase. This is justified by the dynamical properties, such as the mean square displacements and self-diffusion coefficients presented in the following part of the article. Mg ions penetrate into the first coordination shell of unlike ions (Mg–P) due to their higher mobility. The penetration of Mg ions results with a shift of the first peak position of unlike ions to a shorter distance with increasing temperature. It becomes more distinct during the melting. Moreover, it is marked that the first and second coordination shells of Mg–Mg and P–P merge into a single broader peak due to more pronounced thermal vibrations with increasing temperature.

Table 3. The first and second close contact distance and coordination numbers of Mg_3P_2 at 300 K.

Ion pair	1st CCD (Å)	2nd CCD (Å)	1st CN	2nd CN
Mg–Mg	3.25	4.05	4	8
Mg–P	2.55 (2.54–2.64)	4.95	4 (4)	12
P–P	4.05	4.45	6	6

Data in brackets are taken from the first principles calculations [2].

The radial distribution functions $g_{ij}(r)$ of hypernetted-chain approximate theory of liquid state calculations are also presented in Figure 5 at $T_f = 1050$K and $T_f = 1300$K and compared with the MD simulation results. The HNC calculations have been carried out by cooling down the system gradually from the initial temperature $T_i = 5000$K to the final thermodynamic states of temperature $T_f = 1050$K and the number density $n = 0.0276$ ion/Å^3, and $T_f = 1300$K and the number density $n = 0.0256$ ion/Å^3. The HNC results also exhibit distinctive features of a binary ionic liquid and, in general, are in fairly good agreement with the MD simulation results at both temperatures except for the notable discrepancies at short range for Mg–Mg pair, and slight difference in the height and the position of the principal peaks of Mg-P and P–P pairs. These shortcomings of the hypernetted-chain approximation arise due to the assumption made on the bridge function $B_{ij}(r)$ in the exact closure of liquid state theories [7]. The internal energy per particle of a two-component liquid can be obtained from

$$\frac{E}{N} = \frac{3}{2}k_B T + \frac{n}{2}\sum c_i c_j \int g_{ij}(r)\phi_{ij}(r)d^3\vec{r} \qquad (4)$$

where n and c_{ij} are the number density and the number concentrations, respectively. The internal energies per ion at 1050 K are estimated as −7.50 eV from the HNC calculations using Equation (4) and −7.75 eV from the MD simulation.

The average first and second close contact distance between the ions (CCD) and the estimated number of particles in the first and second coordination shells at 300 K are listed in Table 3. The Mg-P separation and the number of P atoms in

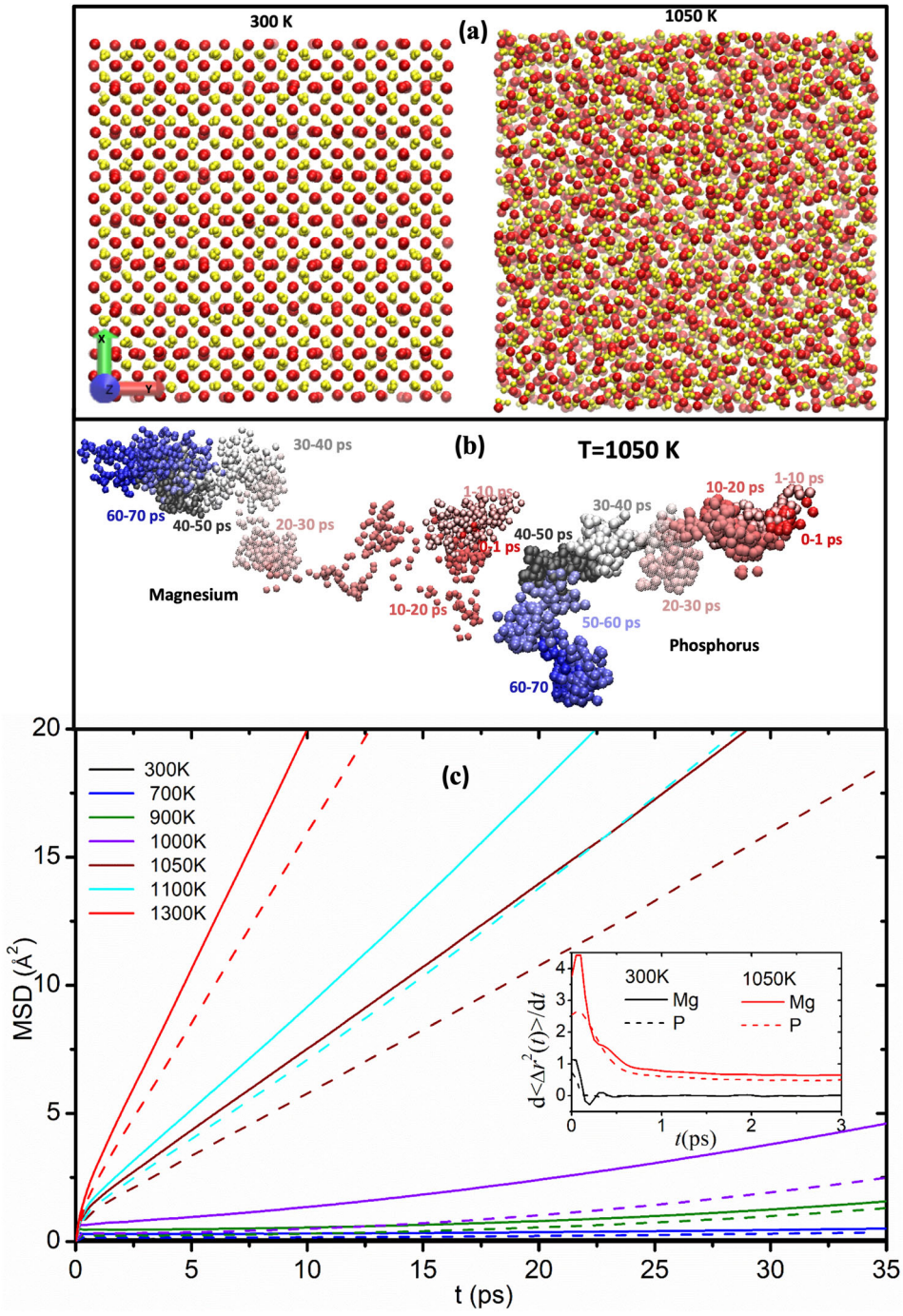


Figure 6. (Colour online) (a) The snapshots of the simulation box at 300 and 1050 K, magnesium and phosphorus ions are represented by yellow and red balls, respectively; (b) The trajectories of magnesium (smaller balls on the left) and phosphorus (larger balls on the right) ions at 1050 K during 70 ps, each colour represents different time intervals; (c) The MSD versus time is plotted for Mg (solid lines) and P (dashed lines) ions at seven different temperatures. The inset is the first derivative of the MSD with respect to time at 300 and 1050 K.

the first coordination shell of each Mg atom agree with the previous first principles calculations for $Ia\bar{3}$ structure at zero pressure given in brackets in the Table 3 [2].

Understanding the self-ionic diffusion and mobility mechanism of ionic materials is of particular importance in electrochemical applications. Such properties correspond to time correlation function the mean square displacement MSD, $\langle \Delta r^2(t) \rangle$, which calculates the average distance of ionic species at equilibrium at time t apart, and is regardless of the time origin. The short time ($t \rightarrow 0$) and long time ($t \rightarrow \infty$) asymptotic limits of the MSD function, respectively, determine the ballistic and diffusive movement of the particles. Figure 6(a) is the snapshots of the simulation box at 300 K and 1050 K which clearly demonstrate the order and disorder of magnesium (yellow ions) and phosphorus (red ions) substructures at solid and liquid phases. Figure 6(b) shows the trajectories of magnesium (on the left) and phosphorus (on the right) ions at 1050 K during 70 ps. Self-diffusion of each ion visualised by recording the displacements every 0.05 ps with different

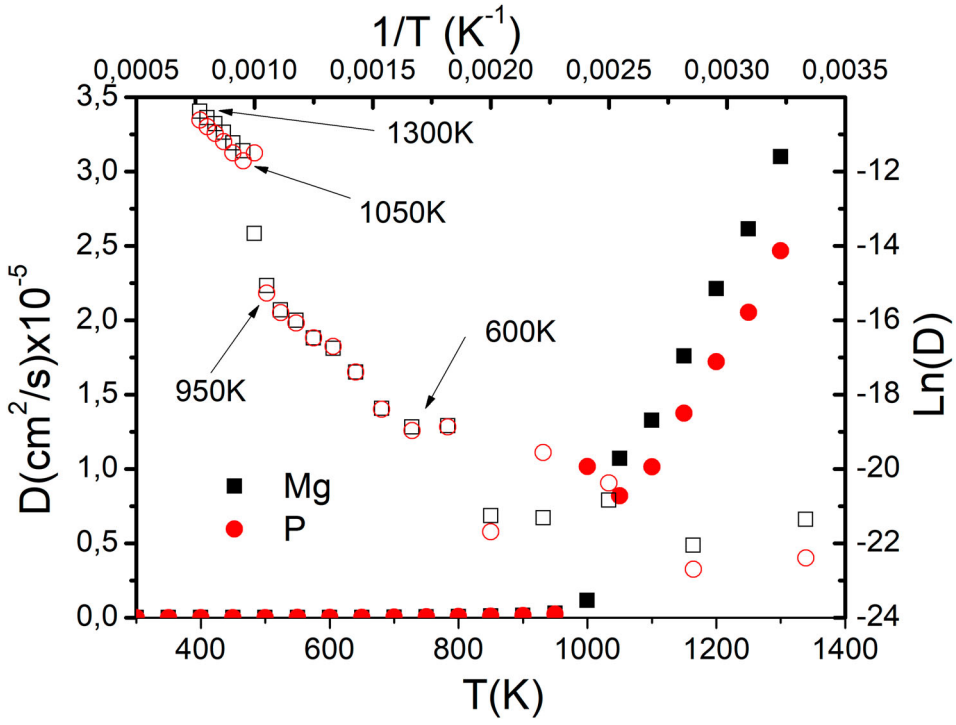


Figure 7. (Colour online) The Einstein self-diffusion coefficients (T) and the Arrhenius plot of diffusion coefficients Ln($D(1/T)$) of magnesium and phosphorus ions

colours for the following time intervals; 0–1 ps red balls, 1–10 ps opaque light-pink balls, … , 60–70 ps opaque dark-blue balls. It is evident that the magnesium ion (smaller balls) exhibits more diffusive behaviour than the phosphorus ion (larger balls). The MSD versus time is plotted for Mg (solid lines) and P (dashed lines) ions at seven different temperatures in Figure 6(c). At a long time scale, almost zero asymptotic slopes of MSDs of both species up to about almost 1050 K means that the two sublattices constructed Mg and P ions are at the solid state. Beyond 1050 K, it is evident from the linear change of the MSD that both ionic components are at the diffusive regime and the system is at molten phase. The ballistic motion of the ions is presented at the short-time region. The derivative of the MSD, which is proportional with the time-dependent diffusion coefficient, at solid (300 K) and liquid phase (1050 K) is shown as inset in Figure 6 (c) in order to see diffusive behaviour in detail. At the solid phase, both ions are at ballistic regime during the time ≤ 0.7ps, and beyond that they exhibit zero diffusion. Whereas, at 1050 K both ions experience constant diffusive behaviour after the rattling motion within the cage formed by the neighbouring ions during the time scale ≤ 1.0ps. Estimated value of the melting temperature 1050 K from the dynamical properties reasonably agrees with the literature value of $>$ 1023K [15,16].

Self-diffusion coefficients D_{Mg} and D_{P} can be estimated from the long-time behaviour of the MDS as it is the geometrically slope of the straight line, $D_i = \lim_{t\to\infty} \frac{\Delta r_i^2(t)}{6t}$ which are plotted against temperature and shown by filled black square (D_{Mg}) and filled red circle (D_{P}) in Figure 7. Both cation and anion exhibit almost zero diffusion up to $\sim$ 1000K then rapid increase at about 1050 K that indicates thermally induced transition of Mg_3P_2 from solid to liquid phase. At the liquid phase, a normal self-diffusion behaviour is observed, namely an exponential increase, by the both ions.

The Arrhenius law can be used to describe the temperature dependence of the diffusion mechanism; $D_i(T) = D_0 \exp(-\Delta H_i/k_B T)$, where ΔH_i is the activation enthalpy for the diffusion process. The Arrhenius graph of Mg (empty black squares) and P (empty red circles) ions is shown in Figure 7. There exist two different temperature range that ions obey the Arrhenius behaviour of the diffusion is obvious at two regions, just before the melting between 600K-950 K and after the melting 1050–1300 K, where it linearly varies with temperature and the slope gives the activation energies. Estimated activation energies of the ions for the diffusion process are $\Delta H_{\mathrm{Mg}} = 0.53$eV and $\Delta H_P = 0.51$eV at solid, and $\Delta H_{\mathrm{Mg}} = 0.51$eV and $\Delta H_P = 0.53$eV at liquid (Figure 7).

The transference number t_i is defined as the ratio of the self-diffusion coefficient of an ion to the total diffusion coefficient within the Nernst–Einstein frame work. In the Arrhenius regime at solid the transference numbers of cation and anion are almost equal $t_{\mathrm{Mg}} \approx t_{\mathrm{P}} \cong 0.5$. Whereas, because of the slightly more diffusive behaviour of the Mg ions at liquid the cation transference number is also slightly greater than that of anions, $t_{\mathrm{Mg}} \cong 0.56$ and $t_{\mathrm{P}} \cong 0.44$.

4. Conclusion

Magnesium phosphide Mg_3P_2 is a potential candidate material for thermoelectronic and optoelectronic device development due to its the structural, electronic, optical and thermoelectric properties. Molecular dynamics simulation and hypernetted-chain approximation calculations were performed for Mg_3P_2

between 300 and 1500 K, and at 1050 K, respectively, using a newly developed classical interatomic potential of Buckingham type. It is concluded that the developed model potential successfully describes the characteristic features of the static and dynamical properties of Mg_3P_2 at solid and liquid phases: the lattice constant, bulk modulus, cohesive energy, X-ray powder diffraction pattern, the radial distribution functions, coordination numbers, mean square displacements, self-diffusion coefficients and transition temperature. Although the results presented in this work is not directly related to the thermoelectronic and optoelectronic properties, the achievement of structural stability and knowledge on diffusion of ions over a wide range of temperature plays nevertheless important role in the thermoelectronic, optoelectronic and energy storage applications.

Acknowledgments

The authors would like to acknowledge that this paper is submitted in partial fulfilment of the requirements for PhD degree at Yildiz Technical University.

Disclosure statement

No potential conflict of interest was reported by the author(s).

References

[1] Ullah M, Murtaza G, Ramay SM, et al. Structural, electronic, optical and thermoelectric properties of Mg3X2 (X = N, P, As, Sb, Bi) compounds. Mater Res Bull. 2017;91:22–30. doi:10.1016/j.materresbull.2017.03.012

[2] Liu B, Hao J, Tang X, et al. Pressure-induced phase transformations in Mg_3P_2 from first- principles calculations. J Alloys Compd. 2017;720:207–211. doi:10.1016/j.jallcom.2017.05.265

[3] Pöhls JH, Faghaninia A, Petretto G, et al. Metal phosphides as potential thermoelectric materials. J Mater Chem C. 2017;5:12441–12456. doi:10.1039/C7TC03948D

[4] Imai Y, Watanabe A. Electronic structures of Mg_3Pn_2 (Pn = N, P, As, Sb and Bi) and Ca_3N_2 calculated by a first-principle pseudopotential method. J Mater Sci. 2006;41:2435–2441. doi:10.1007/s10853-006-5181-3

[5] The Materials Project. (2020). Materials data on Mg_3P_2 by materials project. USA: N. p. Web. doi:10.17188/1200521.

[6] Wyckoff RWG. Crystal structures. Vol 2. 2nd edn New York, London: Sydney Interscience Publishers; 1964.

[7] Allen MP, Tildesley DJ. Computer simulation of liquids. New York (NY): Oxford University Press; 1987.

[8] Berendsen HJC, Postma JPM, van Gunsteren WF, et al. Molecular dynamics with coupling to an external bath. J Chem Phys. 1984;81:3684–3690. doi:10.1063/1.448118

[9] Hansen JP, McDonald IR. The theory of simple liquids. New York (NY): Academic; 1986.

[10] Gillan MJ. A new method of solving the liquid structure integral equations. Mol Phys. 1979;38(6):1781–1794. doi:10.1080/00268977900102861

[11] Abernethy GM, Gillan MJ. A new method of solving the HNC equation for ionic liquids. Mol Phys. 1980;39(4):839–847. doi:10.1080/00268978000100721

[12] Fumi FG, Tosi MP. Ionic sizes and born repulsive parameters in the NaCl-type alkali halides—II: The generalized huggins-mayer form. J Phys Chem Solids. 1964;25(1):45–52. doi:10.1016/0022-3697(64)90160-X

[13] Gale JD, Rohl AL. The general utility lattice program (GULP). Mol Simul. 2003;29(5):91–341.

[14] Refson KA KA. Portable molecular dynamics simulation program for serial and parallel computers. Comput Phys Commun. 2000;126(3):310–329. doi:10.1016/S0010-4655(99)00496-8

[15] ChemicalBook.com [Internet]. Albany (NY); [cited 2006]. Available from: https://m.chemicalbook.com/ProductMSDSDetailCB5191154_EN.htm.

[16] International Programme on Chemical Safety: IPCS. INCHEM: Chemical safety information from intergovernmental organizations. Geneva, Switzerland: World Health Organization, Canadian Centre for Occupational Health and Safety. Inter-Organization Programme for the Sound Management of Chemicals. (2018). Available from: https://inchem.org/documents/icsc/icsc/eics0744.htm.

[17] Momma K, Izumi K. VESTA 3 for three-dimensional visualization of crystal, volumetric and morphology data. J Appl Crystallogr. 2011;44:1272–1276. doi:10.1107/S0021889811038970